AZO embedded interdigitated electrodes for monitoring stimuli responsive materials

Nerea Gil-González,[1,2] Chaoqiu Chen,[3] T. Akyazi,[4] A. Zuzuarregui,[3] A. Rodriguez,[1,2] M. Knez,[3,5] E. Castaño,[1,2] F. Benito-Lopez,[4] M.C. Morant-Miñana[3,]*

[1] Ceit, Manuel Lardizabal 15, 20018 Donostia / San Sebastián, Spain

[2] Universidad de Navarra, Tecnun, Manuel Lardizabal 13, 20018 Donostia / San Sebastián, Spain

[3] CIC nanoGUNE, Tolosa Hiribidea, 76, 20018, Donostia-San Sebastián, Spain

[4] Analytical Microsystems & Materials for Lab-on-a-Chip (AMMa-LOAC) Group, Microfluidics Cluster UPV/EHU, Analytical Chemistry Department, University of the Basque Country UPV/EHU, Vitoria-Gasteiz, Spain

[5] IKERBASQUE, Basque Foundation for Science, Maria Diaz de Haro 3, 48013 Bilbao, Spain

e-mail corresponding: mc.morant@nanogune.eu

Abstract

A combination of atomic layer deposition and photolithography was applied to fabricate interdigitated electrodes of aluminium-doped zinc oxide on polyethylene terephthalate

substrates. Various designs with different gap widths were realized and important characteristic of the electrodes, including thickness, surface roughness and electrical properties with different $ZnO:Al_2O_3$ ratios were studied. Oxygen plasma was applied to etch the polyethylene terephthalate surface and to embed the electrodes, a methodology which is a breakthrough towards ultimately thin devices fabrication. Moreover the influence of oxygen plasma on the electrical properties of aluminum-doped zinc oxide was analyzed. Electrochemical impedance spectroscopy studies of two different stimuli responsive ionogels were performed using the fabricated electrodes as a proof of concept of the viability of these electrodes. The results show the suitability of the use of these fabricated electrodes to monitor changes in ion motion and morphology of stimuli responsive materials. These electrodes and the process of characterization of the ionogels presented here couldbe implemented to monitor electrochemical changes in real applications such as protective coatings.

Keywords: Aluminum-doped zinc oxide, atomic layer deposition, oxygen plasma, ionogels, interdigitated electrodes

Introduction

Combining thin transparent conducting oxide (TCO) films with polymeric substrates is an appealing approach towards realizing thinner, lighter and cheaper devices, such as remote control circuits [1], organic light-emitting devices [2], dye-sensitized solar cells [3], transparent electrodes for touch panels or mobile devices [4]. Indium tin oxide (ITO) is commonly used as TCO. However, several factors such as toxicity [5], low availability shortage and the resulting increase in cost [6], or poor adhesion to organic and polymeric materials [7] trigger investigations for suitable alternatives. Alumina-doped zinc oxide (AZO) is proposed as a promising alternative to ITO since it is cost-efficient for large-

scale applications [5], has a high optical transmittance (T ≥85%) [8], is not toxic [9] and can be grown at relatively low-temperatures [1]. The electrical, optical and structural properties, however, strongly depends on the processing technology, deposition parameters and the ratio of the two constituting materials. AZO films obtained by sputtering have an optical transmittance and electrical resistivity of $2x10^{-4}$ Ω·cm, which are comparable to ITO films ($1x10^{-4}$ Ω·cm) [10]. The lower resistivity in comparison to ZnO ($4x10^{-3}$ Ω·cm) films results from the n-doping of ZnO by Al ions. However, AZO films prepared by magnetron sputtering below 300 ºC show considerable non-uniformities in the resistivity distribution. Further techniques, such as electroless deposition or metalorganic chemical vapor deposition, also require high temperatures to obtain homogeneous films with large areas of low resistivities [11]. More recently, optimization of the doping concentration and processing conditions resulted in AZO films with low resistivities [12–17], even on flexible substrates [18]. Atomic layer deposition (ALD) is a very well suitable technique to fabricate uniform AZO films with resistivities down to $7x10^{-4}$ Ω·cm, even on substrates with sizes of few m^2 and with complicated morphologies [19]. This method is based on a sequential introduction of two or more precursors and intermittent purging steps that in the course of the process grow the desired film in a self-terminating and precisely controlled layer-by-layer fashion, with Angstrom-scale precision in thickness [20]. It has been suggested that the increase in conductivity observed from ALD-grown films is a consequence of the oxygen vacancies and zinc interstitials formed after the incorporation of the Al atoms into the ZnO matrix [16].

Although ALD provides AZO films with great chemical stability, the poor adhesion between the ALD layer and the substrate still poses a challenge. The films can easily delaminate or at least scratch upon mechanical interaction. An alternative approach

relies on embedding into and anchoring of the electrodes to polymers, which avoids the wipe-off of the electrodes and results in mechanically and chemically more stable devices [21]. Moreover, this approach suppresses the formation of scratches and cracks and allows for the design of more compact and thinner devices.

For applications in small and integrated devices, patterning of continuous films with high accuracy and enhanced resolution, without compromising the conductivity and the transmittance of the ALD layer, is of great importance. However, only few examples of direct patterning of ALD thin films into specific geometries can be found in literature. Area-selective atomic layer deposition (AS-ALD) relies on a patterning method in which a growth inhibitor is patterned onto the substrate prior to ALD, thus the deposition will only occur on unblocked regions [22]. For such localized inhibition, PDMS stamps have been inked with molecules that form self-assembled monolayers (SAMs) and transferred to a substrate by microcontact printing (μ-CP). Consequently, the SAMs on the substrate inhibited binding of the precursors and the growth of HfO_2, Pt [23,24] or ZnO [25] layers by ALD. However, a drawback of this technique is the lateral increase in size of the patterns when the height of the growing film at the boundary of patterned and unpatterned regions exceeds the height of the SAMs (*ca.* 2nm) [26]. This will affect the fabrication of patterns in which the width of the structures is a critical parameter, such as, interdigitated electrodes (IDEs). Moreover, it has been observed that diffusion of ALD precursors through SAMs films causes undesired nucleation even in growth-inhibited regions. This limitation of the SAMs can be circumvented by using polymers as inhibitors for an ALD growth [27], especially if used as sufficiently thick defect-free masking layer [28]. For example, polymethacrylamide (PMAM) patterned by μ-CP has been used as resist for AS-ALD of platinum [29] and polymethyl methacrylate (PMMA) patterned by AFM nanotlithography for AS-ALD of TiO_2 [30]. Inkject-printed

patterns of poly(vinyl pyrrolidone) (PVP) have been developed to locally inhibit AZO growth [31]. In an indirect approach, lift-off processes upon photo- or electron beam lithography have been proven as a useful approach for obtaining sharp step edges in patterned ALD films of dielectric layers such as Al_2O_3, ZrO_2 or HfO_2 on silicon substrates [32]. Compared to sputtered or evaporated films, these films are superior in continuity, smoothness, conformability and achievable feature size. Therefore, researchers make use of the structural properties of the ALD-AZO films but none of them exploit its electrical or electrochemical properties to build devices that, for instance, could be employed to detect changes on a polymer layer coated onto them. These changes can be/could be related with the integrity of the coating so, to monitor coating performance over time could minimize maintenance and reparation costs. Electrochemical Impedance Spectroscopy (EIS) with interdigitated electrodes (IDEs) provides a means of monitoring a protective coating, being an interesting approach for monitoring protective coatings.

In this paper, we demonstrate a simple and reliable method to fabricate AZO-IDEs embedded in polyethylene terephthalate (PET) substrates. The fabrication method of these electrodes combines of photolithographic techniques and ALD in a smart way. Subsequent lift-off results in interdigitated finger electrodes of various widths and gap ratios. Etching of the polymeric substrate with oxygen (O_2) plasma enables an integration of AZO-IDEs into the PET. The resulting devices have been used, as a proof of concept, to monitor changes in response to an aqueous environment of organic coatings based on ionogels (IOs), which are polymer gels incorporating an ionic liquid (IL) into their matrices [33], when deposited over the electrodes. The IO conformational changes of two different IO were successfully monitored trough the changes in charge-

transfer resistance (R_{CT}) measured and characterized with the transparent AZO-IDEs patterned onto PET substrates.

Experimental

Reagents and Materials

The masks used for the photolithographic process were manufactured by Microlithographic Services. Trimethylaluminum and diethylzinc were purchased from Strem Chemicals. *N*-isopropylacrylamide, *N,N'*-methylene-bis(acrylamide), 2,2-Dimethoxy-2-phenylacetophenone, 1-ethyl-3-methylimidazolium ethyl sulfate, trihexyltetradecyl-phosphonium dicyanamide ionic liquids and 2,2´-azino-bis-(3-ethylbenzothiazoline-6-sulfonic acid (ABTS) were purchased from Sigma-Aldrich. Cyclic olefin copolymer (COP) was provided by Zeonex/Zeonor and pressure sensitive adhesive (PSA) was generously provided by Adhesive Research, Ireland. Polyethylene terephthalate (PET) was generously provided by Osram. For the photolithography process Microposit S1818 G2 positive photoresist, Microposit developer and Microposit remover 1165 were purchased from Chemplate Materials.

Preparation of the ionogel solutions

The synthesis of the IOs was performed following the protocol described in reference [34]. In brief a mixture of *N*-isopropylacrylamide (0.904 g), *N,N'*-methylene-bis(acrylamide) (0.025 g), 2,2-Dimethoxy-2-phenylacetophenone (0.021 g) and 2 mL of 1-ethyl-3-methylimidazolium ethyl sulfate (IO-1) or trihexyltetradecyl-phosphonium dicyanamide (IO-2) ionic liquid was placed in a flask and heated at 80 °C during 30 min. The chemical structures of the IOs used in this study are shown in the supporting information (Figure SI-1).

Fabrication of the device and ionogel integration

The AZO-IDEs were fabricated on a commercial sheet of polyethylene terephthalate (PET) wafer with a very smooth surface. For the patterning of the embedded interdigitated electrodes, PET substrates were coated with S1818 photoresist and exposed to UV light through a photomask. The exposed regions were removed with Microposit developer. PET substrates covered with the patterned photoresist were treated with O_2 plasma at 100 W during 5 min to improve the adhesion of the deposited AZO films. The AZO layers were grown by ALD (Beneq TFS 200) using diethylzinc (DEZ) and water vapor as zinc and oxygen sources. For the doping process with aluminum, trimethylaluminum (TMA) and water vapor pulses were added to the ALD process. The reactor pressure during the process was 0.7 mbar and the nitrogen purging gas flow rate was 200 sccm. The substrate temperature during ALD was kept at 120 ºC and various $ZnO:Al_2O_3$ ratios were tested. After the ALD process takes place, the photoresist was removed with Microposit 1165 remover and the AZO-IDEs were ultrasonically cleaned using acetone and ethanol. A second O_2 plasma treatment was applied after the fabrication of the AZO-IDEs to study the effect of the O_2 on the AZO resistance.

To integrate the IO into the fabricated device, a COP/PSA gasket with a square shape inside with dimensions of 1.4 x 1 mm was placed around the AZO-IDEs to avoid the spreading of the IO before the photopolymerization (see figure SI-1). Next 1 μL of IO-1 or IO-2 was drop casted onto the AZO-IDEs and *in-situ* photo-polymerized under UV light (λ = 350 nm) with a power of 850 μWcm^{-3} during 8 min. For the optical measurements a 4 mM of ABTS solution in water was used. For monitoring the IO with

AZO-IDEs, the IO was dried in vacuum for 2 h (IO-1) or overnight (IO-2) and subsequently rehydrated with water during 5 min (IO-1) or 15 min (IO-2).

Characterization methods

A JPK NanoWizard atomic force microscope (AFM) was employed to study the topography of the AZO-IDEs. It was operated in the intermittent contact mode using a silicon tip ($r < 10$ nm) with a resonant frequency of approximately 300 kHz and a force constant of 40 Nm^{-1}. The EIS measurements were performed with a Hioki IM3570 impedance analyzer in the frequency window of 4 Hz to 1 MHz. The electrodes were connected with needles controlled by micropositioners. The data was fitted with an equivalent circuit using Z_{view} to quantitatively analyze the results. I-V curves were measured with a Keithley 4200-SCS Semiconductor Characterization System. The thickness of the AZO layer was measured by X-ray reflectivity (XRR). A Pico Plasma System (low-pressure plasma) manufactured by Diener Electronics, was used for O_2 plasma treatments. Thicknesses of the micropatterns and etching depth were measured with a profilometer from KLA-Tencor Technologies. Scanning Electron Microscopy (SEM) was performed with a FEI Quanta 250 FEG to acquire micrographs of the embedded AZO-IDEs and patterned PET. The chemical composition of the films was analyzed by Energy Dispersive X-ray Spectroscopy (EDS) using a field emission scanning electron microscope (JEOL JSM-7100F). The optical transmission was measured using a nanodrop 2000C UV−Visible spectrophotometer (Ocean Optics).

Results and discussion

Fabrication of the AZO-IDEs

Transparent conducting electrodes with excellent electrical and optical properties were fabricated by a merger of photolithographic structuring and ALD thin film growth. The fabrication process has been adapted from protocols described in literature [35] and is schematically outlined in figure 1a. In a typical process, the substrate was spin-coated (figure 1 a-2) with a positive photoresist, subsequently exposed to UV light through a photomask to transfer the interdigitated pattern (figure 1 a-3) and the exposed photoresist was then removed by dissolution (figure 1 a-4). O_2 plasma treatment (figure 1 a-5) was applied to the substrate on the one hand to form of reactive sites for the chemical binding of the AZO layer and on the other hand to etch the unprotected regions of the PET substrates and in this way to generate the trenches for embedding the AZO films. In the following process, the AZO layer was grown by ALD (figure 1 a-6) and the photoresist gently dissolved, leaving behind the bare AZO layer completely embedded in the PET film (figure 1 a-7).

Earlier work has shown that the resistivity of the AZO films grown onto silicon substrates decreases with increasing process temperature [36]. Considering the melting point of the PET (T_m = 250 °C) and the thermal stability of the photoresist used for the patterning of the ALD films, we chose a process temperature of 120 ºC. The number of ALD cycles was adjusted to obtain films with thicknesses of approximately 50 nm. However, the adhesion of the AZO layer to the PET substrate was poor and the film was full of cracks (see figure SI-2) due to the difference in the thermal expansion coefficients of the two involved materials and the brittleness of the AZO film. Oxygen (O_2) plasma has been demonstrated as a viable means to improve the adhesion of ALD layers of TiO_2 to polymeric substrates such as FEP [37]. Similar O_2 plasma treatment of the PET substrates and subsequent deposition of the AZO layer resulted in a more stable coating with no appreciable defects. In addition, the adhesion of the AZO films to the

PET substrates was significantly improved when the substrates were treated with plasma O_2 prior to an ALD deposition. The plasma activates the surface of the PET substrate and introduces O_2. As a result, the chemical bonding between the substrate and the ALD layer becomes stronger.

To study the effect of ZnO to Al_2O_3 pulse ratio on the film resistance, the ALD process temperature was maintained at 120 ºC and the pulse ratio was varied from 10:1 to 30:1 (see table 1). The total number of cycles (440) was maintained constant among the different samples, which due to different growth rates of the Al_2O_3 and ZnO resulted in the thicknesses of the films varying from 50 to 54 nm in dependence of the pulse ratios (see table 1). The results of the current-voltage (I-V) curves measured on PET substrates as a function of pulse ratio are shown in figure S3. As can be seen in table 1, in the range of pulse ratios studied in this work, the resistance values vary from 0.59 MΩ to 2.47 MΩ. According to other works reported in the literature [14,16,38], as the doping occurs via the incorporated Al atoms, almost the same number of charged donors is formed at or near the ZnO/Al_2O_3 interphase. Consequently, the resistance decreases until the interval of Al_2O_3 layers reaches length (ratio 20 to 1 to our study). Shorter distances between two adjacent Al_2O_3 layers could produce repulsion between the Al^{3+} ions occupying the Zn^{+2} lattice sites limiting the extrinsic doping and explaining the increase in resistance at a 10:1 ratio. Consequently, a certain number of ZnO deposition cycles is needed between adjacent Al_2O_3 layers to allow for the nucleation and growth of ZnO and to fully activate the extrinsic doping of ALD-AZO films. Therefore, the ZnO:Al_2O_3 ratio of 20:1 appears to generate the optimal distance between Al_2O_3 layers and a decrease in the AZO resistance.

Further insight into the presence of various conduction processes inside the AZO films was derived from EIS measurements. The recorded Nyquist plots of the AZO

films are shown in figure S3b. The spectra exhibit one semicircle instead of the 2, which would be expected for a semiconductor, indicating that either the conduction process through the grain and the grain boundary has the same time constants, or that resistive grain boundaries and conducting grain cores are present in on the AZO films [39]. The semicircle of the Nyquist plot was fitted with the equivalent circuit shown in the inset of the figure S3 where R_1 stands for the resistance of the connections and $R_2||C$ the conduction through the AZO layer. The estimated resistances listed in table 1 agree well with the values obtained from the I-V plots.

Table 1. Fabrication conditions of AZO-IDEs on PET.

Entry	T (°C)[(a)]	ZnO:Al_2O_3 ratio	Thickness (nm)[(b)]	RMS-Roughness (nm)[(c)]	Diameter (nm)[(d)]	R (Ohms)[(e)]	R_2 (Ohms)[(f)]
1	120	10:1	54	1.4 ± 0.7	48 ± 17	$1.78x10^6$	$0.81 \cdot 10^6$
2	120	20:1	50	1.2 ± 0.1	33 ± 12	$5.92x10^5$	$5.98 \cdot 10^5$
3	120	30:1	52	1.1 ± 0.2	45 ± 12	$2.47x10^6$	$2.64 \cdot 10^6$

[(a)]ALD deposition temperature; [(b)]AZO thickness measured by X-ray reflectivity (XRR); [(c)]Root Mean Square (RMS)-roughness measured by AFM; [(d)]AZO grain size from AFM images; [(e)]Resistance from I-V curves; [(f)]Charge-transfer resistance obtained from the fitting the Nyquist plots with the equivalent circuit.

The microstructure of the ALD AZO films has to be characterized since this parameter is strongly correlated with the electrical properties. To study the film morphology, AZO layers were deposited onto silicon (100) substrates and their surface grain structure was analyzed by AFM. Topographical images of the films with ZnO:Al_2O_3 ratios of 10:1, 20:1 and 30:1 are shown in figure 1b to 1d. Obviously, the morphologies vary with different ZnO:Al_2O_3 ratios. From these images, the RMS-average diameters of the grains were measured and are listed in table 1. Interestingly,

the RMS-roughness and the measured grain size are approximately the same in all the samples. Therefore, the changes in conductivity cannot be related to the size and the number of grain boundaries or the difference in roughness between the samples.

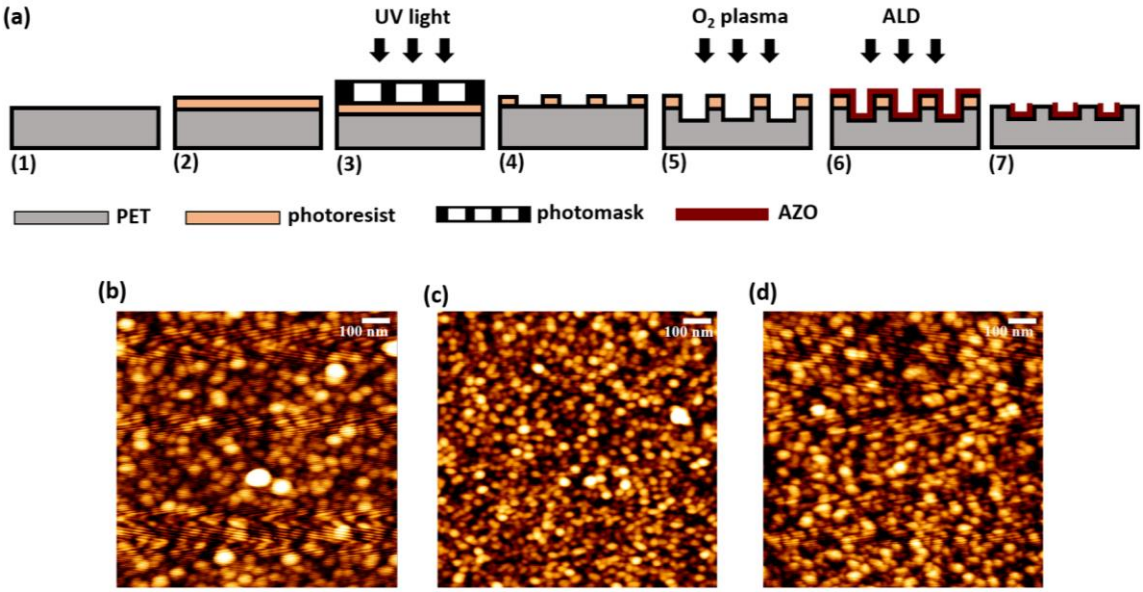

Figure 1. (a) Fabrication process of AZO-IDEs: (1) PET substrate was coated with a (2) photoresist, (3) exposed to UV light through a photomask, (4) developed, (5) exposed to O_2 plasma, (6) AZO was deposited by ALD and (7) the film was immersed in a solvent and photoresist lifted off in that sequence. AFM images of AZO with ZnO:Al_2O_3 ratios of (b) 10:1, (c) 20:1 and (d) 30:1.

Once the AZO deposition process was established, the patterned AZO-IDEs were successfully obtained on the polymer substrate as can be seen in figure 2a. Width to gap ratios of 100:100, 50:50, 25:25 and 50:25 micrometers were fabricated showing the feasibility of the method for fabricating different structures. Scanning electron microscopy (SEM) images performed on the samples (figure 2b, 2c and 2d) demonstrate that the electrodes are well defined and the width of the fingers match perfectly with the geometries defined by the mask. Moreover, the EDS spectra clearly show the presence of Zn and Al in the AZO electrodes. The presence of trenches inside the PET substrates

can be observed from the bird eye view micrograph of figure 2g. The AZO finger is completely embedded in the polymer substrate with an average thickness depth of 216 ± 20 nm calculated after 3 measurements.

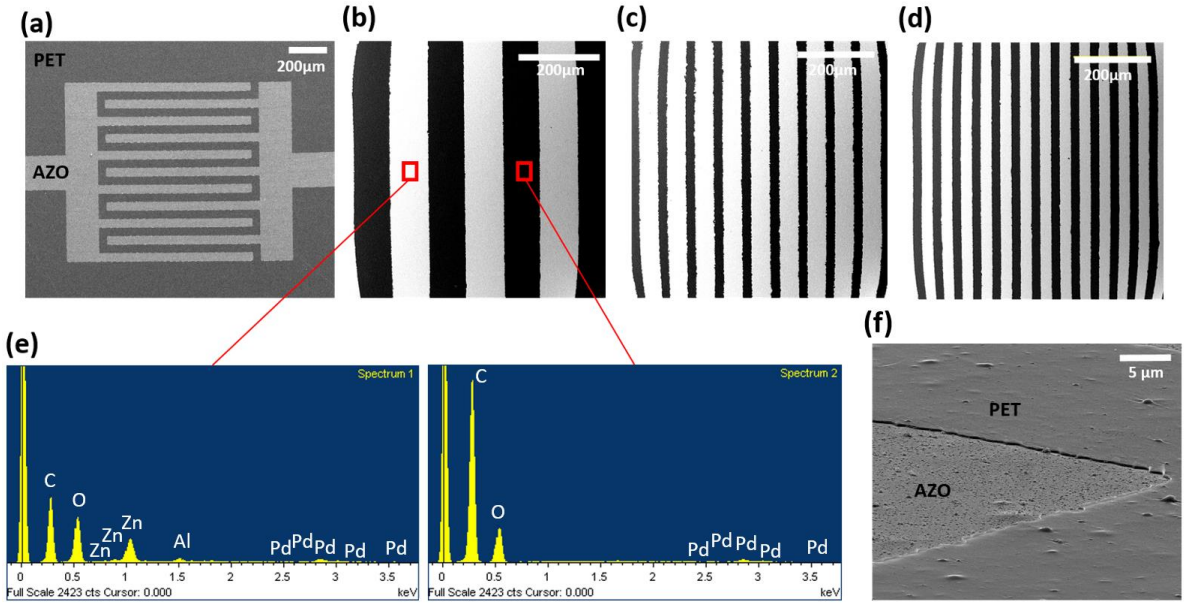

Figure 2.SEM images of AZO-IDEs embedded in PET with a width:gap ratio of (a) 50:50 µm, (b) 100:100, (c) 50:25 and (d) 25:25 µm. EDS spectra of (e) AZO and PET.(f) Birds eye view SEM micrograph of an AZO finger electrode.

The trench formation process was further investigated by changing the O_2 flux and the exposure time in the plasma treatment. The relation of trench depth and exposure time is summarized in Figure 3a. For this experiment, PET foils were covered with a positive photoresist and several lines were patterned by photolithography. O_2 plasma treatments were carried out with gas flows of 5, 10 and 20 sccm at a constant plasma power (100 W). The etching depth was measured every 10 min with a mechanical profilometer (Figure S4). For the three O_2 flows studied, the obtained trend indicates that the trench depth increases almost linearly with the exposure time. However, the differences in slope between the three O_2 flows reflect that lower O_2 flows result in faster etching of the PET substrate. The etch rate decreases with increasing O_2 flow, because at higher

gas pressure the ion energies and the electron densities decrease, suppressing the etching process of the substrate.[40,41] By identifying and controlling these factors, the etch depth in PET films can be well controlled and reproduced making it a simple technique to generate embedded electrodes.

The effect of a second O_2 plasma treatment after the fabrication of the AZO-IDEs on their electronic properties was also studied. For this purpose, 20 min of O_2 plasma with an O_2 flow of 10 sccm was applied to the AZO-IDEs. The Nyquist plots of both O_2-treated and untreated AZO-IDEs are shown in figure SI5. The O_2-treated AZO-IDEs show a smaller semicircle than the untreated electrodes. The resistances (R_2) obtained after fitting both Nyquist plots with the same equivalent circuit, are 0.68 MΩ and 0.12 MΩ before and after O_2 plasma treatment, respectively. The observed decrease in resistance is caused by an increase of the number of charge carriers (electrons) available for conduction [42]. Finally, the mechanical profile of the AZO-IDEs before and after the plasma O_2 was measured, as shown in figure 3b. The substrate regions of the PET, which are not covered by an AZO layer, are more rapidly etched by the O_2 plasma, resulting if an inversion of the morphology with AZO-IDEs acting as etching resist. As a result, the electrodes can be controllably embedded or exposed in dependence on the needs of the anticipated device.

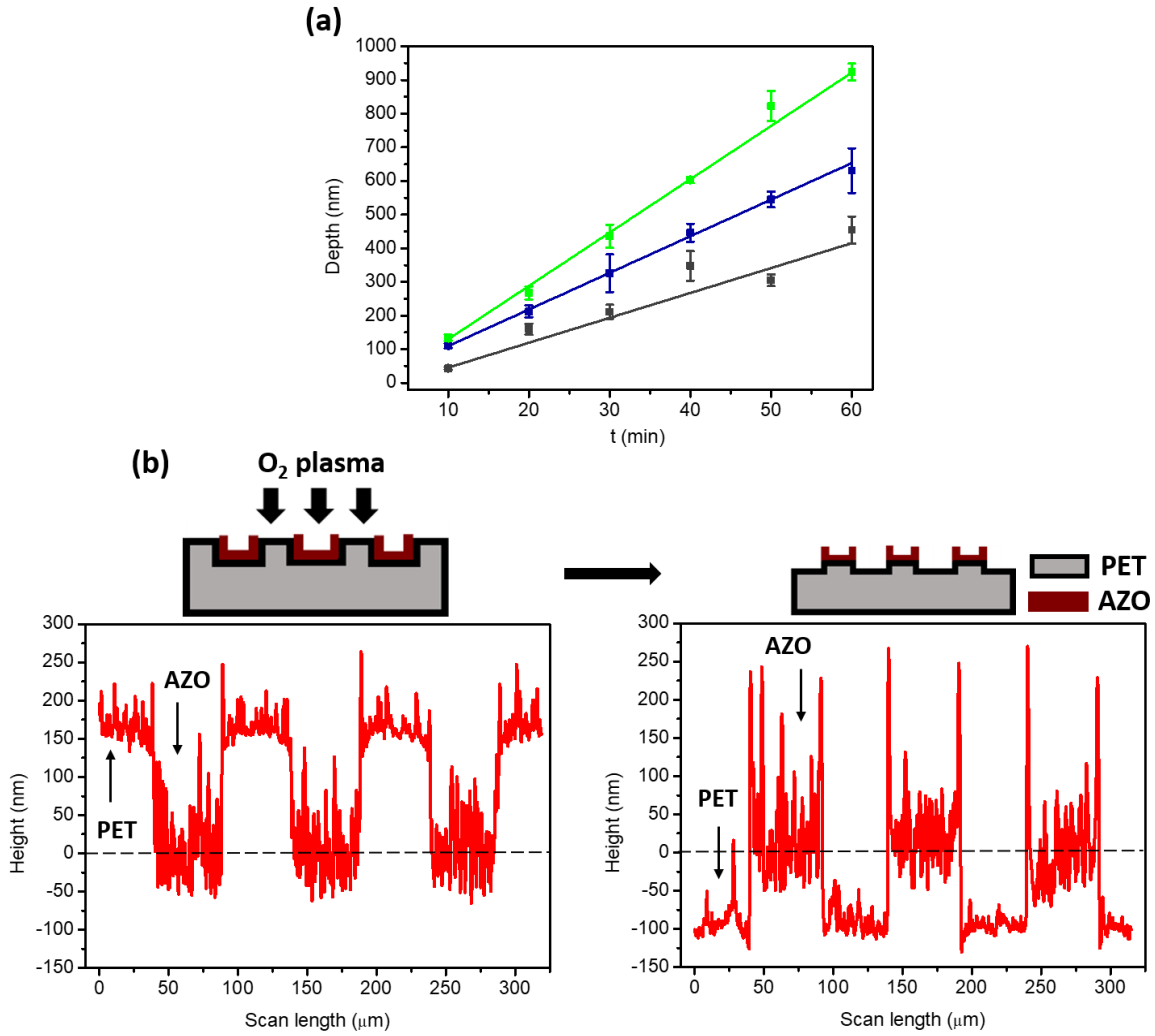

Figure 3. (a) Etching depths of PET by O2 plasma at various O2 flows: 5 sccm (green), 10 sccm (blue), 20 sccm (grey), (n = 3); (b) schematic view and profilometry scans of AZO-IDEs on PET before (left) and after (right) O2 plasma treatment.

Optical characterization of the AZO-IDEs

Optical transparency is an important measure for the quality of the thin TCOs films so the optical transparency of the fabricated AZO-IDEs was evaluated. It is well-known that the visible region of the spectrum of AZO films, the transmittance reaches 80 % over a broad range of wavelengths, which makes a use of these electrodes for optoelectronics applications feasible. The high transmittance of the AZO layer deposited onto PET substrates in the visible region allows to directly measure variations

in the transmission spectra of solutions superpositioned to the AZO-IDEs and electrically stimulated by them. To prove this concept, the oxidation reaction of ABTS induced by electron injection from the AZO electrodes was applied. The colorless ABTS is a chemical compound that can be oxidized to its radical cation ($ABTS^{\cdot+}$) resulting in a green solution [43], see Figure 4a. A drop of the colorless ABTS was placed onto the AZO-IDEs and a bias potential of 7 V was applied to the AZO electrodes during a fixed period of time. The reaction was followed by recording transmittance spectra applying a configuration according to the schematic in figure 4a. Figure 4b shows the transmittance change at 422 nm as a function of time. Before applying the voltage, the recorded transmission spectrum is normalized to 100 % accounting for the contributions of AZO and the PET substrate to the transmittance of the substrate. After applying 7 V for 1 min, oxidation of the ABTS occurs and the transmittance slightly decreases. After 2 min, the transmittance decreases considerably by more than 60 % and after 3 min a drop of 80 % of the initial transmittance is achieved. The results prove that AZO-IDEs fabricated are functioning systems and the optical transparency of the AZO film and the PET substrate allows for direct measurement of the transmittance changes of solutions superpositioned to the electrode in real time.

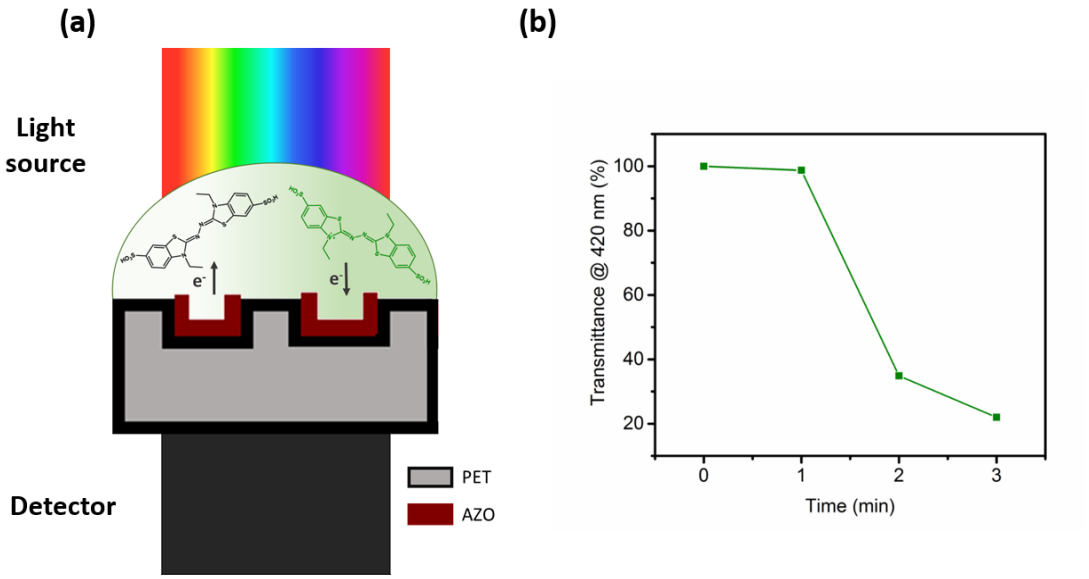

Figure 4. (a) Mechanism of the ABTS oxidation and reduction processes triggered by AZO-IDEs and (b) the evolution of the transmittance % of the ABTS dye as a function of time at 422 nm.

Monitoring of ionogels with AZO-IDEs

The use of AZO-IDEs deposited on PET could be used to monitor the electrochemical changes of materials deposited on top of the electrodes. To prove this concept, stimuli responsive IOs that suffer a conformational change in their structure in aqueous media [44] have been monitored with the previously fabricated AZO-IDEs using EIS. As explained in the experimental section the IO-1 and IO-2 were placed over the electrodes and impedance measurements were performed using the AZO-IDEs with 50 µm gap and width. The spectra show a semicircle at high frequencies and a linear part at low frequencies (see figure S7). Detailed spectra of the high frequency areas are shown in figure 5a. The semicircle is ascribed to the electron transfer process between the IO and the AZO surface and the linear part is characteristic of Warburg diffusion. In the case of IO-1, the semicircle is smaller, which is indicative of the charge-transfer at the AZO/IO-1 interface being more favorable than in case of AZO/IO-2. In order to analyze the

results more quantitatively the equivalent circuit must fit the experimental data of both measured IOs. The equivalent circuit used for this analysis is shown in figure 5b and describes the response of a charge-transfer process accompanied by diffusion. The basic element is represented by R_S and contains the resistance of the electrolyte and the internal resistance of the electrode material. R_{CT} is associated with the charge-transfer between the electrode and the IO and is connected in parallel with the Constant Phase Element (CPE) that corresponds to the double layer. The Warburg impedance (W) accounts for the transport of the IL ions. For both IOs measured with the AZO electrodes we employed the same equivalent circuit and the resulting values allow differentiating between both IOs. The obtained R_{CT} values were 0.62 MΩ and 1.07 MΩ for IO-1 and IO-2, respectively. These differences can be explained with the differing cations of the ILs. In the case of IO-1, the cationic charge of imidazolium is largely delocalized due to the extensive π-bonding in the heterocycle. However, in the case of IO-2, the cationic charge of IL-2 is largely alkyl-shielded [45], restricting the charge-transfer to some extent [44] and resulting in higher R_{CT} values. The R_{CT} values using the AZO-IDEs with lower resistance (treated with O_2 plasma) were 0.2 MΩ and 0.79 MΩ for IO-1 and IO-2, respectively. This decrease in the R_{CT} of the IOs is a consequence of an improved charge-transfer at the IO/AZO interface. These results are in agreement with our previous studies reported by us [46] that proof that EIS correlates changes in the R_{CT} values with the polymer morphology and the nature of the IL entrapped in the matrix. Moreover, they validate the feasibility of AZO-IDEs to distinguish between IOs.

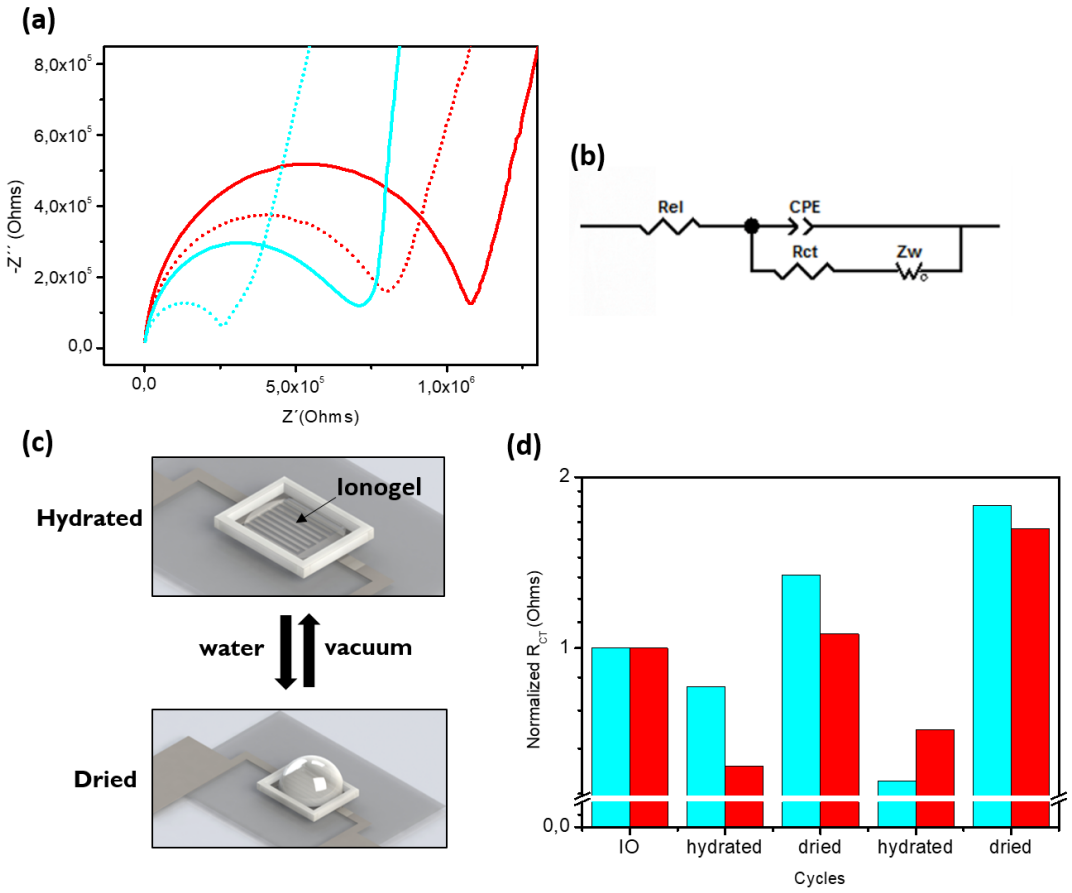

Figure 5. (a) Nyquist plot of IO-1 (blue lines) and IO-2 (red lines) using AZO-IDEs with (dotted lines) and without (solid lines) O_2 plasma treatment. (b) The Randles equivalent circuit used for fitting the plots. (c) Schematic of the device: IO placed on top of an AZO-IDE with a COP/PSA gasket, indicating the reversible swelling of the IO. (d) Normalized R_{CT} values for IO-1 (blue) and IO-2 (red) upon swelling/drying cycles. The cycles consist of treatments of 5 min (IO-1) or 15 min (IO-2) in water and 2 h (IO-1) or overnight (IO-2) in vacuum.

IOs are porous materials that swell in an aqueous environment. Upon absorbing large amounts of water, they change their volume abruptly which induces severe conformational changes in the microstructure, thus affecting their ion mobility [34]. Therefore, our designed AZO-IDEs have been used to monitor such changes by EIS. After polymerization of the IO on top of the AZO-IDEs, the hydrated and dried states

were obtained after immersion in water or drying in vacuum in various durations. The schematics of the setup are depicted in Figure 5c and experimental details are described in the experimental section. EIS measurements were performed in the swollen and dehydrated state and the obtained spectra (see figure SI-8) were fitted with the Randles equivalent circuit shown in figure 5b. The immersion times for rehydrations and drying times for dehydration were adjusted for each IO, based on our earlier work [46].

Both the dehydrated and swollen states are reflected in the normalized (I/I_0) R_{CT} graph shown in figure 5d. The spectra have been normalized to account for differences between the different electrodes. In the swollen state, the R_{CT} of both IOs decreases indicating that the expanded structure of the IO promotes ion mobility. In contrast, after drying in vacuum, the R_{CT} values measured with AZO-IDEs reach higher values, because after water evaporation of water the pores become filled with air, which impedes the charge-transfer between the electrode and the IL. Moreover, differences in the actuating behavior of IO-1 and IO-2 can be elucidated using AZO-IDEs. IO-1 has a spongy structure and the presence of the hydrophilic anion of the IL favors water absorption through the polymer matrix. Therefore, low immersion/drying times are needed to perceive a change in the R_{CT} due to its rapid water uptake and release capacity. In contrast, the compact structure of IO-2 and its hydrophobic anion hinder the water uptake/release and longer times are needed to observe a change in the R_{CT} values. Moreover, water molecules are trapped more efficiently due to the compact morphology of IO-2, resulting in its swollen state being more stable than in the case of IO-1. The rather high values obtained in the last cycle are a consequence of the IOs peeling off of the AZO-IDEs. The experimental shows that variations in ion mobility, generated by conformational changes in the IOs, can be monitored with the fabricated AZO-IDEs, in the same way as it was previously done with gold electrodes. This demonstrates the

feasibility of the implementation of AZO-IDEs to detect failures in protective coatings that involve adhesion deterioration or ion migration processes.

Conclusions

A process to fabricate AZO-IDEs embedded in PET substrates was described. ALD was used as deposition method and the optimal $ZnO:Al_2O_3$ ratio, thickness and temperature were identified. Photolithography and lift-off techniques were used to pattern the AZO film and four devices were fabricated with different width to gap ratios. The procedure allows for advancing the manufacturing of thinner devices and in the patterning of TCOs deposited by ALD.

The electrical properties of the AZO films were characterized by EIS and IV measurements and the AZO resulting from a $ZnO:Al_2O_3$ ALD cycle ratio of 20:1 showed the lowest resistance. The influence of oxygen plasma treatment on the electronic properties of AZO was studied showing a shift towards lower resistance values. Finally, AZO-IDEs were used to monitor the swelling/drying behavior of two different IOs in water. The possible use of AZO-IDE, embedded in flexible substrates, in order to monitor electrochemical changes in IOs related with variations in their microstructure, was successfully proven with EIS. This confirms the feasibility of the method to be implemented in monitoring systems that suffer changes in ion motion, such as protective coatings. A timely detection of structural changes in coatings or detachment or delamination of coatings from a substrate can help to avoid or prevent damages, such as corrosion-related damages, in metallic substrates.

Acknowledgments

This work was supported by the Basque Government under the Elkartek Program (MICRO4FAB, Grant No. KK-2016/00030). Nerea Gil-Gonzalez was supported by a PhD fellowship from the University of Navarra. MCMM acknowledges the Basque Government under the Etortek Program (Grant No. KK-2017/0012). F.B.L. acknowledges the Ramón y Cajal Programme (Ministerio de Economía y Competitividad), the Gobierno Vasco, Dpto. Industria, Innovación, Comercio y Turismo under ELKARTEK KK-2017/00088 and the funding support from Gobierno de España, Ministerio de Economía y Competitividad, with Grant No. BIO2016-80417-P. M.K. acknowledges financial support by the Spanish Ministry of Economy and Competitiveness (MINECO) within grant agreement no. MAT2016-77393-R, including FEDER funds, and the Maria de Maeztu Units of Excellence Programme - MDM-2016-0618. FBL and TA personally acknowledge Marian M. de Pancorbo for letting them use her laboratory facilities at UPV/EHU. MCMM acknowledges Prof Seifert for letting them use his laboratory facilities and Dr. A. Beloqui for helpful discussions.

References

(1) Banerjee, N.; Ghosh, C. K.; Chattopadhyay, K. K.; Minoura, H.; Sarkar, A. K.; Akiba, A.; Kamiya, A.; Endo, T. Low-Temperature Deposition of ZnO Thin Films on PET and Glass Substrates by DC-Sputtering Technique. *Thin Solid Films* **2006**, *496* (1), 112–116.

(2) Yang, C.; Lee, S.; Lin, T.; Chen, S. Electrical and Optical Properties of Indium Tin Oxide Films Prepared on Plastic Substrates by Radio Frequency Magnetron Sputtering. *Thin Solid Films* **2008**, *516* (8), 1984–1991.

(3) Galstyan, V.; Vomiero, A.; Concina, I.; Braga, A.; Brisotto, M.; Bontempi, E.; Faglia, G.; Sberveglieri, G. Vertically Aligned TiO2 Nanotubes on Plastic Substrates for Flexible Solar Cells. *Small* **2011**, *7* (17), 2437–2442.

(4) Facchetti, A.; Marks, T. J. Deposition and Performance Challenges of Transparent Conductive Oxides on Plastic Substrates. In *Transparent Electronics: From Synthesis to Applications*; Facchetti, A., Marks, T. J., Eds.; 2010; pp 103–140.

(5) Lin, Y. C.; Jian, Y. C.; Jiang, J. H. A Study on the Wet Etching Behavior of AZO (ZnO:Al) Transparent Conducting Film. *Appl. Surf. Sci.* **2008**, *254* (9), 2671–2677.

(6) Patel, N. Characterization of Electrical Performance of Aluminum-Doped Zinc Oxide Pellets. *DePaul Discov.* **2014**, *3* (1).

(7) Alemu, D.; Wei, H.-Y.; Ho, K.-C.; Chu, C.-W. Highly Conductive PEDOT:PSS Electrode by Simple Film Treatment with Methanol for ITO-Free Polymer Solar Cells. *Energy Environ. Sci.* **2012**, *5* (11), 9662–9671.

(8) Ellmer, K.; Kudella, F.; Mientus, R.; Shiceck, R.; Fietcher, S. Influence of Discharge Parameters on the Layer Properties of Reactive Magnetron Sputtered ZnO:Al Films. *Thin Solid Films* **1994**, *247* (1), 15–23.

(9) Maldonado, F.; Stashans, A. Al-Doped ZnO: Electronic, Electrical and Structural Properties. *J. Phys. Chem. Solids* **2010**, *71* (5), 784–787.

(10) *Transparent Conductive Zinc Oxide*, 1st ed.; Ellmer, K., Andreas, K., Rech, B., Eds.; Springer-Verlag Berlin Heidelberg, 2008; Vol. 104.

(11) Sato, H.; Minami, T.; Takata, S.; Miyata, T.; Ishii, M. Low Temperature Preparation of Transparent Conducting ZnO:Al Thin Films by Chemical Beam Deposition. *Thin Solid Films* **1993**, *236* (1–2), 14–19.

(12) Lujala, V.; Skarp, J.; Tammenmaa, M.; Suntola, T. Atomic Layer Epitaxy Growth of Doped Zinc Oxide Thin Films from Organometals. *Appl. Surf. Sci.* **1994**, *82–83*, 34–40.

(13) Elam, J. W.; Routkevitch, D.; George, S. M. Properties of ZnO/Al2O3 Alloy Films Grown Using Atomic Layer Deposition Techniques. *J. Electrochem. Soc.* **2003**, *150* (6), G339–G347.

(14) Cheun, H.; Fuentes-Hernandez, C.; Shim, J.; Fang, Y.; Cai, Y.; Li, H.; Sigdel, A. K.; Meyer, J.; Maibach, J.; Dindar, A.; et al. Oriented Growth of Al2O3:ZnO Nanolaminates for Use as Electron-Selective Electrodes in Inverted Polymer Solar Cells. *Adv. Funct. Mater.* **2012**, *22* (7), 1531–1538.

(15) PARK, S.-H. K.; LEE, J.-I.; HWANG, C.-S.; CHU, H. Y. Characteristics of Organic Light Emitting Diodes with Al-Doped ZnO Anode Deposited by Atomic Layer Deposition. *Jpn. J. Appl. Phys.* **2005**, *44* (7), L242–L245.

(16) Lee, D.-J.; Kim, H.-M.; Kwon, J.-Y.; Choi, H.; Kim, S.-H.; Kim, K.-B. Structural and Electrical Properties of Atomic Layer Deposited Al-Doped ZnO Films. *Adv. Funct. Mater.* **2011**, *21* (3), 448–455.

(17) Genevée, P.; Donsanti, F.; Renou, G.; Lincot, D. Study of the Aluminum Doping of Zinc Oxide Films Prepared by Atomic Layer Deposition at Low Temperature. *Appl. Surf. Sci.* **2013**, *264*, 464–469.

(18) Luka, G.; Witkowski, B. S.; Wachnicki, L.; Jakiela, R.; Virt, I. S.; Andrzejczuk, M.; Lewandowska, M.; Godlewski, M. Electrical and Mechanical Stability of Aluminum-Doped ZnO Films Grown on Flexible Substrates by Atomic Layer Deposition. *Mater. Sci. Eng. B* **2014**, *186*, 15–20.

(19) Luka, G.; Krajewski, T. A.; Witkowski, B. S.; Wisz, G.; Virt, I. S.; Guziewicz, E.; Godlewski, M. Aluminum-Doped Zinc Oxide Films Grown by Atomic Layer Deposition for Transparent Electrode Applications. *J. Mater. Sci. Mater. Electron.* **2011**, *22* (12), 1810–1815.

(20) Knez, M.; Nielsch, K.; Niinistö, L. Synthesis and Surface Engineering of Complex Nanostructures by Atomic Layer Deposition. *Adv. Mater.* **2007**, *19* (21), 3425–3438.

(21) Khan, A.; Lee, S.; Jang, T.; Xiong, Z.; Zhang, C.; Tang, J.; Guo, L. J.; Li, W.-D. High-Performance Flexible Transparent Electrode with an Embedded Metal Mesh Fabricated by Cost-Effective Solution Process. *Micro Nano No Small Matter* **2016**, *12* (22), 3021–3030.

(22) Jiang, X.; Bent, S. F. Area-Selective Atomic Layer Deposition of Platinum on YSZ Substrates Using Microcontact Printed SAMs. *J. Electrochem. Soc.* **2007**, *154* (12), D648–D656.

(23) Jiang, X.; Bent, S. F. Area-Selective ALD with Soft Lithographic Methods: Using Self-Assembled Monolayers to Direct Film Deposition. *J. Phys. Chem. C* **2009**, *113* (41), 17613–17625.

(24) Jiang, X.; Huang, H.; Prinz, F. B.; Bent, S. F. Application of Atomic Layer Deposition of Platinum to Solid Oxide Fuel Cells. *Chem. Mater.* **2008**, *20* (12),

3897–3905.

(25) Yan, M.; Koide, Y.; Babcock, J. R.; Markworth, P. R.; Belot, J. A.; Marks, T. J.; Chang, R. P. H. Selective-Area Atomic Layer Epitaxy Growth of ZnO Features on Soft Lithography- Patterned Substrates. *Appl. Phys. Lett.* **2001**, *79* (11), 1709–1711.

(26) Ras, R. H. A.; Sahramo, E.; Malm, J.; Raula, J.; Karppinen, M. Blocking the Lateral Film Growth at the Nanoscale in Area-Selective Atomic Layer Deposition. *J. Am. Chem. Soc.* **2008**, *130* (34), 11252–11253.

(27) Sinha, A.; Hess, D. W.; Henderson, C. L. Transport Behavior of Atomic Layer Deposition Precursors through Polymer Masking Layers: Influence on Area Selective Atomic Layer Deposition. *J. Vac. Sci. Technol. B, Nanotechnol. Microelectron. Mater. Process. Meas. Phenom.* **2007**, *25*, 1721.

(28) Sinha, A.; Hess, D. W.; Henderson, C. L. Area-Selective ALD of Titanium Dioxide Using Lithographically Defined Poly(methyl Methacrylate) Films. *J. Electrochem. Soc.* **2006**, *153* (5), G465–G469.

(29) Mullings, M. N.; Lee, H.-B.-R.; Marchack, N.; Jiang, X.; Chen, Z.; Gorlin, Y.; Lin, K.-P.; Bent, S. F. Area Selective Atomic Layer Deposition by Microcontact Printing with a Water-Soluble Polymer. *J. Electrochem. Soc.* **2010**, *157* (12), D600–D604.

(30) Hua, Y.; King, W. P.; Henderson, C. L. Nanopatterning Materials Using Area Selective Atomic Layer Deposition in Conjunction with Thermochemical Surface Modification via Heated AFM Cantilever Probe Lithography. *Microelectron. Eng.* **2008**, *85* (5–6), 934–936.

(31) Ellinger, C. R.; Nelson, S. F. Selective Area Spatial Atomic Layer Deposition of ZnO, Al2O3, and Aluminum-Doped ZnO Using Poly(vinyl Pyrrolidone). *Chem. Mater.* **2014**, *26* (4), 1514–1522.

(32) Biercuk, M. J.; Monsma, D. J.; Marcus, C. M.; Becker, J. S.; Gordon, R. G. Low-Temperature Atomic-Layer-Deposition Lift-off Method for Microelectronic and Nanoelectronic Applications. *Appl. Phys. Lett.* **2003**, *83* (12), 2405.

(33) Akyazi, T.; Gil-González, N.; Basabe-Desmonts, L.; Castaño, E.; Morant-Miñana, M. C.; Benito-Lopez*, F. Manipulation of Fluid Flow Direction in Microfluidic Paper-Based Analytical Devices with an Ionogel Negative Passive Pump. *Sensors Actuators B Chem.* **2017**, *247*, 114–123.

(34) Akyazi, T.; Saez, J.; Elizalde, J.; Benito-Lopez, F. Fluidic Flow Delay by Ionogel Passive Pumps in Microfluidic Paper-Based Analytical Devices. *Sensors Actuators, B Chem.* **2016**, *233*, 402–408.

(35) Rojo, L.; Castro-Hurtado, I.; Morant-Miñana, M. C.; Mandayo, G. G.; Castaño, E. Enhanced Features of Li2CO3 Induced by Thickness and Annealing Time. *CrystEngComm* **2015**, *17*, 1597–1602.

(36) Gong, S. C.; Choi, Y.-J.; Kim, H.; Park, C.-S.; Park, H.-H.; Jang, J. G.; Chang, H. J.; Yeom, G. Y. Aluminum-Doped Zinc Oxide Formed by Atomic Layer Deposition for Use as Anodes in Organic Light Emitting Diodes. *J. Vac. Sci. Technol. A Vacuum, Surfaces, Film.* **2013**, *31* (1), 01A101.

(37) Zuzuarregui, A.; Coto, B.; Rodríguez, J.; Gregorczyk, K. E.; Ruiz de Gopegui, U.; Barriga, J.; Knez, M. Highly Reflective Polymeric Substrates Functionalized Utilizing Atomic Layer Deposition. *Appl. Phys. Lett.* **2015**, *107* (6), 61602.

(38) Na, J.-S.; Scarel, G.; Parsons, G. N. In Situ Analysis of Dopant Incorporation , Activation , and Film Growth during Thin Film ZnO and ZnO:Al Atomic Layer Deposition. *J. Phys. Chem.* **2010**, *114* (1), 383–388.

(39) Suganya, L.; Sundaresan, B.; Sankareswari, G.; Ravichandran, K.; Sakthivel, B. Influence of Incorporation of Al3+ Ions on the Structural, Optical and AC Impedance Characteristics of Spin Coated ZnO Thin Films. *J. Mater. Sci. Mater. Electron.* **2014**, *25* (1), 361–368.

(40) Hartney, M. A.; Greene, W. M.; Soane, D. S.; Hess, D. W. Effects of Ion Bombardment in Oxygen Plasma Etching. In *Proceedings SPIE 0920, Advances in Resist Technology and Processing V*; 1988; Vol. 920.

(41) Riekerink Olde, M. B. Structural and Chemical Modification of Polymer Surfaces By Gas Plasma Etching, Universiteit Twente, 2001.

(42) Kim, J. S.; Cacialli, F.; Cola, A.; Gigli, G.; Cingolani, R. Increase of Charge Carriers Density and Reduction of Hall Mobilities in Oxygen-Plasma Treated Indium-Tin-Oxide Anodes. *Appl. Phys. Lett.* **1999**, *75* (1), 19–21.

(43) Re, R.; Pellegrini, N.; Proteggente, A.; Pannala, A.; Yang, M.; Rice-Evans, C. Antioxidant Activity Applying an Improved Abts Radical Cation Decolorization Assay. *Free Radic. Biol. Med.* **1999**, *26* (9/10), 1231–1237.

(44) Gil-González, N.; Akyazi, T.; Zuzuarregui, A.; Castaño, E.; Benito-Lopez, F.; Morant-Miñana, M. C. Understanding the Behavior of Stimuli-Response Ionogels for Microfluidic Applications. In *Procedia Engineering*; 2016; Vol. 168, pp 473–476.

(45) Kavanagh, A.; Copperwhite, R.; Oubaha, M.; Owens, J.; McDonagh, C.; Diamond, D.; Byrne, R. Photo-Patternable Hybrid Ionogels for Electrochromic Applications. *J. Mater. Chem.* **2011**, *21* (24), 8687.

(46) Gil-González, N.; Akyazi, T.; Castaño, E.; Benito-Lopez, F.; Morant-Miñana, M. C. Elucidating the Role of the Ionic Liquid in the Actuation Behavior of Thermo-Responsive Ionogels. *Sensors Actuators B Chem.* **2018**, *260*, 380–387.